Signal Processing 141 (2017) 57–73

Contents lists available at ScienceDirect

Signal Processing

journal homepage: www.elsevier.com/locate/sigpro

New discrete orthogonal moments for signal analysis

Barmak Honarvar Shakibaei Asli [a], Jan Flusser [a,b,*]

[a] Institute of Information Theory and Automation, Academy of Sciences of the Czech Republic, Pod vodárenskou věží 4, 182 08 Praha 8, Czech Republic
[b] Faculty of Management, University of Economics, Jindřichuv Hradec, Czech Republic

ARTICLE INFO

Article history:
Received 4 November 2016
Revised 19 May 2017
Accepted 23 May 2017
Available online 30 May 2017

Keywords:
Orthogonal polynomials
Moment functions
Z-transform
Rodrigues formula
Hypergeometric form

ABSTRACT

The paper addresses some computational aspects and applications of the polynomial unbiased finite impulse response functions originally derived by Shmaliy as a new class of a one-parameter family of discrete orthogonal polynomials. We present two new explicit formulas to compute these polynomials directly. They are based on the discrete Rodrigues' representation and hypergeometric form, respectively. These straightforward calculations lead us to propose another discrete signal representation in moment domain. Experimental results show a comparison between the proposed moments and discrete Chebyshev moments in terms of noise-free/noisy signal feature extraction and reconstruction error.

1. Introduction

Although orthogonal polynomials over discrete sets were considered as early as the middle of the nineteenth century by Chebyshev [1–3], relatively little attention had been paid to them until now. They appear naturally in discrete moment theory, statistics and various areas of digital signal and image processing such as object recognition, speech and image reconstruction, and invariant analysis. Thereafter, such polynomials have been applied to solve a wide range of 1D and 2D signal processing problems. In digital communication systems, the discrete orthogonal polynomials (DOPs) play an important role in the efficient approximation of multivariate signals. Later, various classical DOPs, such as Meixner, Hahn, Krawtchouk, Charlier, and Racah polynomials, were presented in a generalized form [2]. These polynomials have a lowering and raising operator, which give rise to a Rodrigues' formula and an explicit expression in terms of hypergeometric form, from which the coefficients of the three-term recurrence relation can be obtained.

There are several efficient applications based on DOPs in the field of signal and image processing. Discrete moment analysis is one of the most widely used techniques to recognize and recover speech signals and images. As follows from [4], the DOPs in the Chebyshev and Krawtchouk moments form can enhance noisy speech signals. The DOPs are also used in image compression [5], speech coding [6], image restoration [7], image analysis and invariants [8]. Mukundan et al. showed that the implementations of continuous moments (such as Zernike, Legendre and Fourier-Mellin moments) involve two main sources of errors including the discrete approximation of the continuous integrals and mapping of the image coordinate system into the area of orthogonality of the polynomials [3,9]. They employed the discrete Chebyshev moments for image analysis and observed they are superior to the continuous moments in terms of image reconstruction capability under the noise-free and noise conditions. Chebyshev moments are based on the discrete Chebyshev polynomials with a single parameter which depends on the data length of N samples. In contrast to the three-parameter Hahn DOPs and two-parameter Krawtchouk DOPs, Shmaliy [10] developed the one-parameter discrete polynomial unbiased finite impulse response (UFIRs) for FIR filters [11–13] referring to the one-step predictive FIRs by Heinonen and Neuvo [14]. Later, Morales-Mendoza et al. showed in [15] that the UFIRs [10] establish a new class of DOPs having a single tuning parameter N (data length) and applied these DOPs in [16] to blind fitting of finite data. An image reconstruction method based on the aforementioned UFIR DOPs has been patented in 2014 [17]. The authors of this patent concluded that such UFIR transform is suitable for real-time processing.

In this paper, we first recall the DOPs derived by Shmaliy as a new class of a single-parameter family of DOPs. Then we propose two different explicit equations to compute these DOPs directly based on the discrete Rodrigues' formula and hypergeometric representation, respectively. The rest of the paper is organized as follows. In Section 2, we review the polynomial signal model and its orthogonality property based on the norm and weight functions. General properties of new DOPs are investigated in

* Corresponding author.
E-mail addresses: honarvar@utia.cas.cz (B.H. Shakibaei Asli), flusser@utia.cas.cz (J. Flusser).

http://dx.doi.org/10.1016/j.sigpro.2017.05.023
0165-1684/

Section 3 including recursive representation, Rodrigues' formula and hypergeometric form. In Section 4, the definition of new DOP as moment function and its inversion formula is discussed. We compare the proposed DOP with its continuous version called radial Mellin in limit condition. Some experimental results in 1D signal reconstruction are presented in Section 5. Section 6 contains concluding remarks.

2. A new class of DOPs

P. Heinonen and Y. Neuvo introduced a new class of FIR-Median Hybrid (FMH) filters which contain linear FIR substructures to estimate the current signal value using forward and backward prediction [14]. It has been shown in [10,15] that the polynomial UFIRs derived by Shmaliy are orthogonal and represent a new class of one-parameter family of one-parameter family of DOPs.

The pth degree discrete Shmaliy polynomial is defined as

$$h_p(n,N)=\sum_{i=0}^{p}a_{ip}(N)n^i, \tag{1}$$

existing from 0 to $N-1$ and having the coefficients a_{ip} defined as

$$a_{ip}(N)=(-1)^i\frac{M^{(p)}_{(i+1),1}(N)}{|H_p(N)|} \tag{2}$$

where $|H_p(N)|$ is the determinant and $M^{(p)}_{(i+1),1}(N)$ is the minor of Hankel matrix $H_p(N)$

$$H_p(N)=\begin{pmatrix} c_0 & c_1 & \cdots & c_p \\ c_1 & c_2 & \cdots & c_{p+1} \\ \vdots & \vdots & \ddots & \vdots \\ c_p & c_{p+1} & \cdots & c_{2p} \end{pmatrix}. \tag{3}$$

The elements of Hankel matrix (3) are power series

$$c_k(N)=\sum_{i=0}^{N-1}i^k=\frac{1}{k+1}(B_{k+1}(N)-B_{k+1}), \tag{4}$$

where $B_k(x)$ is the Bernoulli polynomial and $B_k=B_k(0)$ is the Bernoulli number. By substituting (2) into (1), we obtain a polynomial of a discrete variable n as

$$h_p(n,N)=\sum_{i=0}^{p}(-1)^i\frac{M^{(p)}_{(i+1),1}(N)}{|H_p(N)|}n^i, \tag{5}$$

which is valid for $n=0,1,\ldots,N-1$.

2.1. Some properties of new discrete polynomials

In [16], Morales-Mendoza et al. proved the following fundamental properties of the discrete polynomials (5).

Unit area:

$$\sum_{n=0}^{N-1}h_p(n,N)=1. \tag{6}$$

Zero moments:

$$\sum_{n=0}^{N-1}n^q h_p(n,N)=0,\quad 1\le q\le p. \tag{7}$$

Finite energy:

$$\sum_{n=0}^{N-1}h_p^2(n,N)=a_{0p}<\infty. \tag{8}$$

A class of discrete polynomials $h_p(n,N)$ is orthogonal on $n\in[0,N-1]$. They satisfy the relation

$$\sum_{n=0}^{N-1}w(n,N)h_p(n,N)h_q(n,N)=\rho(p,N)\delta_{pq}, \tag{9}$$

where $p,q=0,1,..,N-1$ and δ_{pq} is the Kronecker symbol. The norm $\rho(p,N)$ of $h_p(n,N)$ is given by [16]:

$$\begin{aligned}\rho(p,N)&=\frac{p+1}{N(N+1)}\prod_{i=0}^{p}\frac{N-i-1}{N+i}\\&=\frac{(p+1)(N-p-1)_p}{N(N)_{p+1}},\end{aligned} \tag{10}$$

where $(a)_0=1,(a)_k=a(a+1)\ldots(a+k-1)$ is the Pochhammer symbol. Weight function $w(n,N)$ is a discrete linear (with respect to n) function

$$w(n,N)=\frac{2n}{N(N-1)}. \tag{11}$$

Note that $w(n,N)$ is not symmetric. This is a substantial difference from other discrete polynomials such as Chebyshev, Krawtchouk and Hahn, the weight functions of which are all symmetric.

The low-degree Shmaliy's DOPs are [10]

$$h_0(n,N)=\frac{1}{N}, \tag{12a}$$

$$h_1(n,N)=\frac{-6n+2(2N-1)}{N(N+1)}, \tag{12b}$$

$$h_2(n,N)=\frac{30n^2-18(2N-1)n+3(3N^2-3N+2)}{N(N+1)(N+2)}, \tag{12c}$$

$$\begin{aligned}h_3(n,N)=&\frac{-140n^3+120(2N-1)n^2}{N(N+1)(N+2)(N+3)}\\&-\frac{20(6N^2-6N+5)n+8(2N^3-3N^2+7N-3)}{N(N+1)(N+2)(N+3)}.\end{aligned} \tag{12d}$$

To achieve numerical stability, a set of weighted proposed polynomials is introduced in this subsection. Therefore, in addition to normalizing the polynomials with the norm, the square root of the weight is also introduced as a scaling factor. Weighted discrete polynomials are defined by

$$\bar{h}_p(n,N)=h_p(n,N)\sqrt{\frac{w(n,N)}{\rho(p,N)}}. \tag{13}$$

For the weighted polynomials, the orthogonality condition in (9) becomes

$$\sum_{n=0}^{N-1}\bar{h}_p(n,N)\bar{h}_q(n,N)=\delta_{pq}. \tag{14}$$

The new ordinary and weighted discrete polynomials up to the third degree for $N=50$ are shown in Fig. 1(a) and (b), respectively.

3. General properties of $h_p(n,N)$

In this section, we analyze the computational aspects of the new discrete polynomials, $h_p(n,N)$, discuss their properties and develop some new ones.

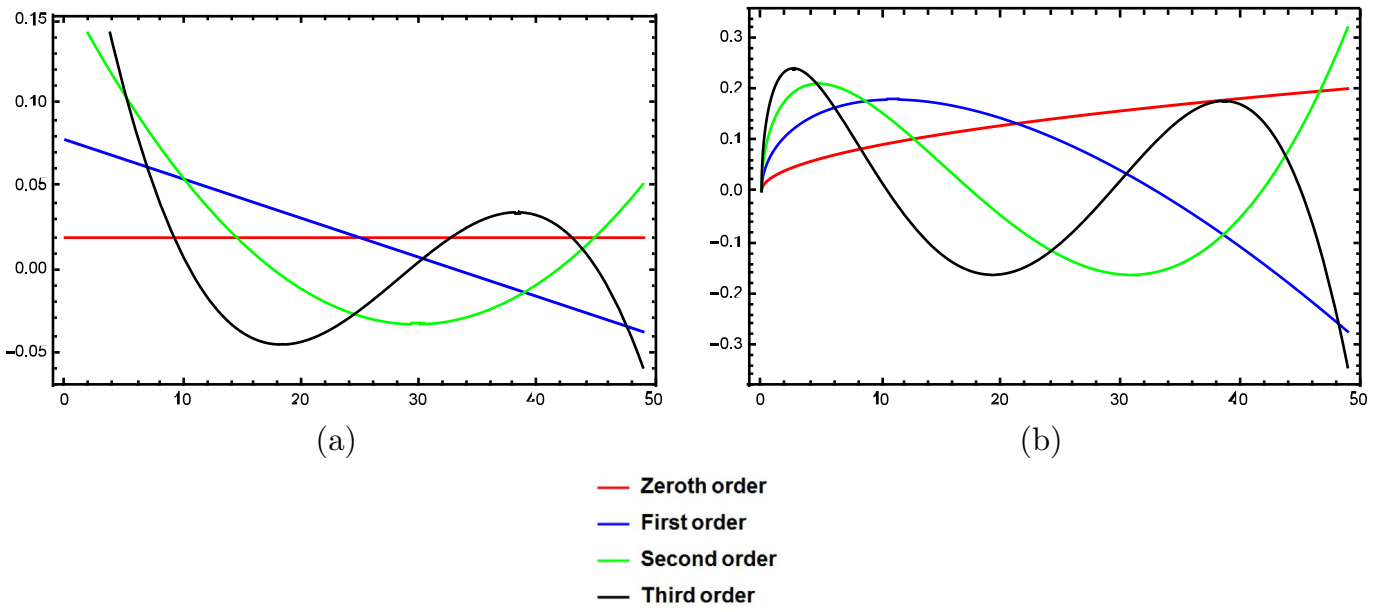

Fig. 1. The plots of the new discrete polynomials for $N = 50$ up to the 3rd degree: (a) ordinary polynomials $h_p(n, N)$ and (b) weighted polynomials $\tilde{h}_p(n, N)$.

3.1. Representation based on the weight function moments

The DOPs $h_p(n, N)$ can be expressed in terms of the kth moments $m_k(N)$ of the weight function $w(n, N)$. The moments are defined as

$$m_k(N) = \sum_{n=0}^{N-1} n^k w(n, N). \tag{15}$$

Assuming $m_k \triangleq m_k(N)$, it is possible to simplify m_k for $k \geq 0$ as [16]

$$m_k = \frac{2}{N(N-1)(k+2)}[B_{k+2}(N) - B_{k+2}(0)]. \tag{16}$$

Now, the set of orthogonal polynomials $h_p(n, N)$ can be represented as

$$h_p(n, N) = r_p(N) \det \boldsymbol{M}, \tag{17}$$

where $r_p(N)$ obeys the unit area property in (6) and

$$\boldsymbol{M} = \begin{pmatrix} m_0 & m_1 & \cdots & m_p \\ m_1 & m_2 & \cdots & m_{p+1} \\ \vdots & \vdots & \ddots & \vdots \\ m_{p-1} & m_p & \cdots & m_{2p-1} \\ 1 & n & \cdots & n^p \end{pmatrix}. \tag{18}$$

3.2. Recursive representation

In [16], Morales-Mendoza et al. showed that orthogonal polynomials $h_p(n, N)$ satisfies the following three-term recurrence relation:

$$p(2p-1)(N+p)h_p(n, N) - 2\left[p^2(2N-1) - n(4p^2-1)\right] \times h_{p-1}(n, N) + p(2p-1)(N-p)h_{p-2}(n, N) = 0, \tag{19}$$

where $p \geq 1$, $h_{-1}(n, N) = 0$ and $h_0(n, N) = \frac{1}{N}$. This recursive implementation can be used for numerical implementation of the polynomials.

3.3. Rodrigues' representation

The continuous orthogonal polynomials such as Legendre, Hermite and Laguerre polynomials may be expressed using Rodrigues' formula [2]:

$$P_n(x) = \frac{1}{r_n w(x)} \frac{\mathrm{d}^n}{\mathrm{d}x^n}\{w(x)g^n(x)\}, \tag{20}$$

where $P_n(x)$ is the continuous polynomial of degree n, $w(x)$ is the weight function, $g(x)$ is a polynomial in x, the coefficients of which are independent of n, and r_n is a coefficient constant with respect to x. An analogous formula exists for DOPs $F_p(n)$, too. We obtain it by replacing the derivatives with forward differences [18] (note that we also replaced the continuous variable x with discrete variable n and the order n with order p for discrete case)

$$F_p(n) = \frac{1}{r_p w(n, N)} \Delta^p\{w(n, N)g(n, p)\}, \tag{21}$$

where Δ is the first-order forward difference

$$\Delta\{f(n)\} = f(n+1) - f(n), \tag{22}$$

Δ^p is the pth order forward difference [19]

$$\Delta^p\{f(n)\} = \sum_{k=0}^{p} (-1)^{p-k} \binom{p}{k} f(n+k), \tag{23}$$

$g(n, p) = g(n)g(n-1)\ldots g(n-p+1)$ such that $g(n)$ is a polynomial in n independent of p and r_p is a constant with respect to n that can be obtained after finding the Rodrigues' representation, as will be shown in (33).

Since the weight function has been known, the only unknown function here is $g(n, p)$. It is rather difficult to find this function in the signal domain. Therefore, we propose transforming Eq. (21) to the Z-domain and find the function $g(n, p)$ there. The left-hand side of (21) equals to the proposed DOP, $h_p(n, N)$. The weight function has a fixed part of $\frac{2}{N(N-1)}$ that can be canceled from the denominator and argument of the forward difference in (21). So, we can rewrite (21) as

$$nh_p(n, N) = \frac{1}{r_p} \Delta^p\{ng(n, p)\}. \tag{24}$$

By applying the Z-transform to (24) with respect to discrete variable n, we get

$$-z\frac{\mathrm{d}H_p(z)}{\mathrm{d}z} = \frac{1}{r_p} Y_p(z) \sum_{k=0}^{p} (-1)^{p-k} \binom{p}{k} z^k, \tag{25}$$

where $H_p(z)$ and $Y_p(z)$ are the Z-transforms of $h_p(n, N)$ and $ng(n, p)$, respectively (see more details in Appendix A). The goal is to find $g(n, p)$ which is related to $y_p(n) \equiv ng(n, p)$ as

$$Y_p(z) = -r_p \frac{z\frac{dH_p(z)}{dz}}{\sum_{k=0}^{p}(-1)^{p-k}\binom{p}{k}z^k}. \tag{26}$$

We set $p = 1$ and get

$$h_1(n, N) = \frac{-6n + 2(2N-1)}{N(N+1)} \overset{\mathscr{Z}}{\longleftrightarrow} H_1(z) = \frac{2z^2(2N-1) - 4z(N+1)}{N(N+1)(z-1)^2},$$

$$\frac{dH_1(z)}{dz} = \frac{8z - 4N(z-1) + 4}{N(N+1)(z-1)^3},$$

and, finally,

$$Y_1(z) = -r_1 \frac{z[8z - 4N(z-1) + 4]}{N(N+1)(z-1)^4}. \tag{27}$$

Applying the inverse Z-transform to (27) yields

$$y_1(n) = \frac{2r_1}{N(N+1)} n(n-1)(N-n). \tag{28}$$

For $p = 1$, we have

$$y_1(n) = ng(n, 1) = ng(n).$$

Therefore, Eq. (28) leads to

$$g(n) = \frac{2r_1}{N(N+1)}(n-1)(N-n) \tag{29}$$

and

$$g(n, p) = \prod_{k=0}^{p-1} g(n-k) = \frac{2r_1}{N(N+1)} \prod_{k=0}^{p-1}(n-k-1)(N-n+k) = \frac{2r_1}{N(N+1)}(n-p)_p(N-n)_p. \tag{30}$$

Note that the solution of the above product can be directly found from the definition of the Pochhammer symbol [20]. By replacing this obtained form of $g(n, p)$ in (24), we arrive at

$$h_p(n, N) = \frac{2r_1}{r_p N(N+1)n} \Delta^p \left\{ n(n-p)_p(N-n)_p \right\}. \tag{31}$$

It is clear that $\frac{2r_1}{r_p N(N+1)}$ is an independent function of n and can be denoted as $\sigma(p, N)$, which yields

$$h_p(n, N) = \frac{1}{n\sigma(p, N)} \Delta^p \left\{ n(n-p)_p(N-n)_p \right\}. \tag{32}$$

By considering the low-order DOPs in Eq. (12), it is easy to find the general form of $\sigma(p, N)$. The process of finding $\sigma(p, N)$ is shown in Appendix B in detail. By replacing this function in (32), we get

$$h_p(n, N) = \frac{p+1}{np!(N)_{p+1}} \Delta^p \left\{ n(n-p)_p(N-n)_p \right\}, \tag{33}$$

which is the discrete case of Rodrigues' formula for representing the discrete polynomials $h_p(n, N)$.

3.4. Hypergeometric representation

The readers can find in [16] the statement, that the representation of polynomials $h_p(n, N)$ via hypergeometric functions has been unknown. Here we present such a representation for the first time.

Theorem 1. *For $p, n, N \geq 0$, the orthogonal discrete polynomials on $[0, N-1]$ defined by (31) satisfy the following relation:*

$$h_p(n, N) = \frac{(-1)^p(p+1)(n-p)_p(N-n)_p}{p!(N)_{p+1}} {}_3F_2(-p, n+1, 1-N+n; n-p, 1-N-p+n; 1). \tag{34}$$

The proof of Theorem 1 is presented in Appendix C.

4. Discrete orthogonal moments of $h_p(n, N)$

Given a set of DOPs $h_p(n, N)$ with weight function $w(n, N)$ and norm $\rho(p, N)$, the orthogonal moment of order $p < N$ of any bounded signal $f(n)$, $n = 1, \ldots, N$, is defined as

$$\mathscr{H}_p = \sum_{n=1}^{N} f(n)\bar{h}_p(n, N+1), \tag{35}$$

where $\bar{h}_p(n, N+1) = h_p(n, N+1)\sqrt{\frac{w(n,N+1)}{\rho(p,N+1)}}$.

Partial reconstruction $\tilde{f}(n)$ of signal $f(n)$ from its moments $\mathscr{H}_p$ up to the order N_{max} can be found as

$$\tilde{f}(n) = \sum_{p=0}^{N_{max}} \mathscr{H}_p \bar{h}_p(n, N+1); \quad n = 1, \ldots, N. \tag{36}$$

Thanks to the orthogonality, if $N_{max} = N-1$, than the reconstructed signal is error-free, which means $\tilde{f}(n) = f(n)$.

The moments as well as the reconstruction can be calculated in a numerically stable way, as will be demonstrated in Section 5. The pseudo code implementation of (35) and (36) is given in Algorithm 1.

Algorithm 1: Algorithm in pseudo code for the implementation of the new discrete orthogonal moments.

Input : Signal $f(n)$, $1 \leq n \leq N$
Output: New discrete moments, $\mathscr{H}_p$ and reconstructed signal, $\tilde{f}(n)$

```
Compute norm, ρ(p, N) and weight, w(p, N) from (10) and (11), respectively
Compute DOPs, h_p(n, N) from (20) or (34)
Compute weighted DOPs, h̄_p(n, N+1) from (13)
for n ← 1 to N do
    for p ← 0 to N − 1 do
        compute ℋ_p from Eq. (35);
    end
end
for p ← 0 to N_max do
    for n ← 1 to N do
        compute f̃(n) from Eq. (36);
    end
end
```

As we can see from the Rodrigues' formula (31) and from the hypergeometric representation (34), there is a close relationship between the proposed discrete polynomials $h_p(n, N)$ and continuous polynomial kernel $Q_p(n)$ (defined on the unit circle) of Fourier-

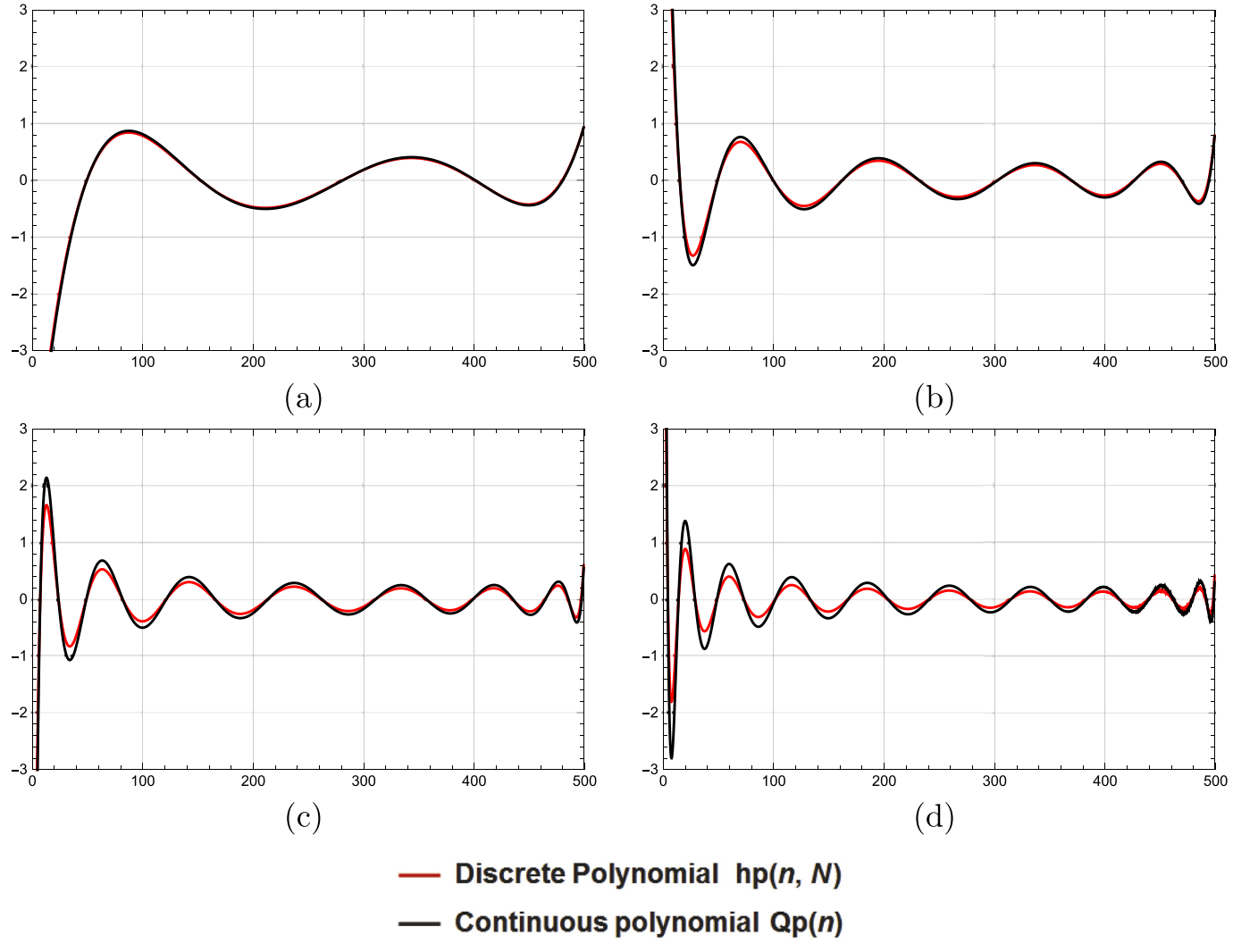

Fig. 2. Comparison between the new discrete polynomials (red) and the continuous radial Mellin polynomials (black) for the (a) 5th degree, (b) 10th degree, (c) 15th degree, and (d) 20th degree.

Mellin transform [21] if N approaches infinity.

$$\lim_{N\to\infty} \frac{N(-1)^p}{p+1} h_p(Nn, N) = Q_p(n), \quad n \in [0,1] \;;\; p = 0, 1, 2, \ldots \tag{37}$$

where

$$Q_p(n) = n^p \binom{2p+1}{p+1} {}_2F_1\left(-p-1, -p; -2p-1; \frac{1}{n}\right). \tag{38}$$

The above fact suggests to perform a comparative analysis between the discrete and continuous polynomials. A comparison plots of $h_p(n, N)$ and radial Mellin polynomials of degrees 5, 10, 15 and 20 are shown in Fig. 2(a), (b), (c) and (d), respectively. In all cases, $N = 500$ was used. We can see from Fig. (2) that for sufficiently large N it is possible to approximate continuous polynomials by discrete ones with a reasonable accuracy.

4.1. Discrete approximation of radial Mellin moments

The errors that are introduced if we apply continuous orthogonal moments to discrete signals can be significant in many applications. As we compared discrete polynomials $h_p(n, N)$ with continuous radial Mellin polynomials $Q_p(n)$ in (37), the definition of continuous radial Mellin moments can be presented as follows:

$$\psi_p = 2(p+1) \int_0^1 f(x) Q_p(x) x \mathrm{d}x. \tag{39}$$

The signal $f(x)$ can be reconstructed from its radial Mellin moments ψ_p using the following formula

$$f(x) = \sum_{p=0}^{\infty} \psi_p Q_p(x), \tag{40}$$

where the upper limit of the summation can be changed, when doing a partial reconstruction, to maximum order of the moments N_{max} similarly to (36). For a 1D signal $f(i)$ of length N, a discrete approximation of (39) is

$$\psi_p = 2(p+1) \sum_{i=0}^{N-1} f(i) \int_{\frac{i}{N}}^{\frac{i+1}{N}} Q_p(x) x \mathrm{d}x. \tag{41}$$

The discretization of continuous integrals as given in (39) affects the orthogonality property of the radial Mellin moments. If

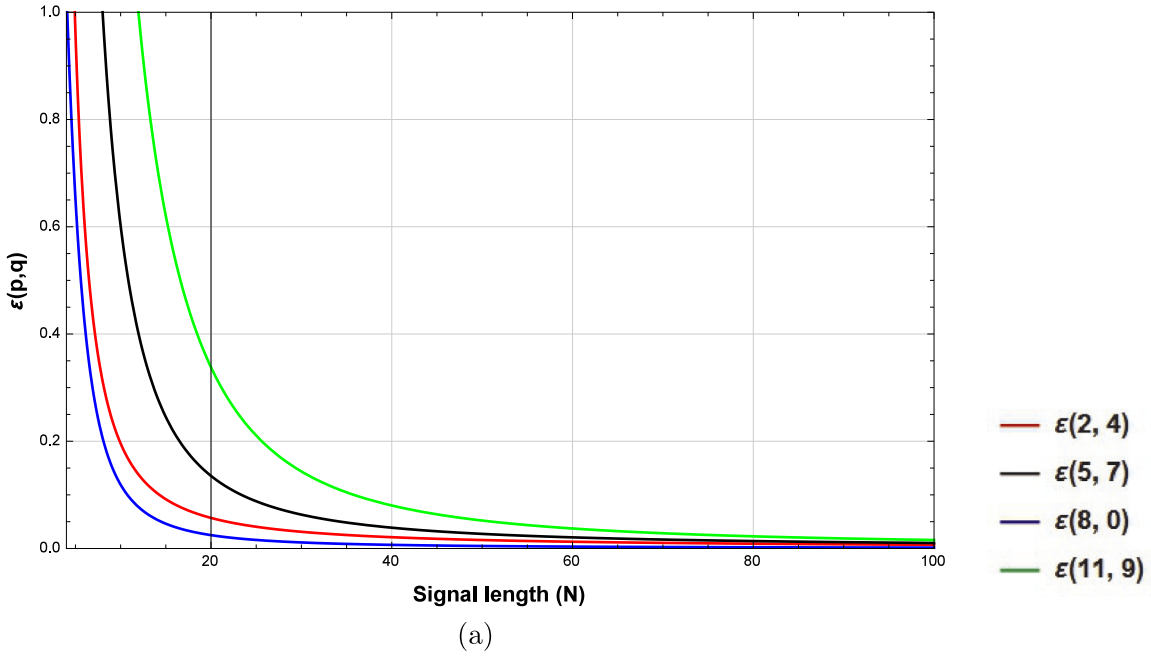

Fig. 3. Orthogonality violation of radial Mellin polynomials due to discretization.

we define

$$\varepsilon(p,q) = \frac{1}{N-1}\sum_{i=0}^{N-1} Q_p(x_i)Q_q(x_i)x_i, \qquad x_i = \frac{i}{N-1}, \tag{42}$$

in the discrete domain of signal, then it is desirable to have $\varepsilon(p,q) = 0$ whenever $p \neq q$. However this condition is not met especially for small values of N. Plots of $\varepsilon(2, 4)$, $\varepsilon(5, 7)$, $\varepsilon(8, 0)$ and $\varepsilon(11, 9)$ with respect to N is shown in Fig. 3. The violation of orthogonality is clearly apparent.

5. Numerical experiments

In this section we illustrate the performance of the proposed moments $\mathscr{H}_p$ in signal reconstruction. We do so for both noise-free and noisy signals and always compare the results with discrete Chebyshev moments, which play the role of "golden standard" in this kind of problems. The comparison has been performed namely in terms of accuracy, which is usually the primary criterion, but we also compared time complexity of both methods.

5.1. The signals

We performed the experiments on six real 1D signals, which were extracted as line segments from the commonly available test image "Baboon". To ensure the diversity of the data, the signals were taken from different parts of the image, see Fig. 4. All extracted signals have the length of 32 samples (see Fig. 5 for the signal plots).

5.2. Noise-free signal reconstruction

In this experiment, we calculated the proposed moments and the discrete Chebyshev moments of the test signals and performed partial reconstruction from moments of orders up to $2, 4, 6, \ldots, 30, 32$ (for the 32nd order the reconstruction becomes complete). The reconstruction process is illustrated in Figs. 6–8 for the signals showed in Fig. 5(a),(c) and (f). We can observe that

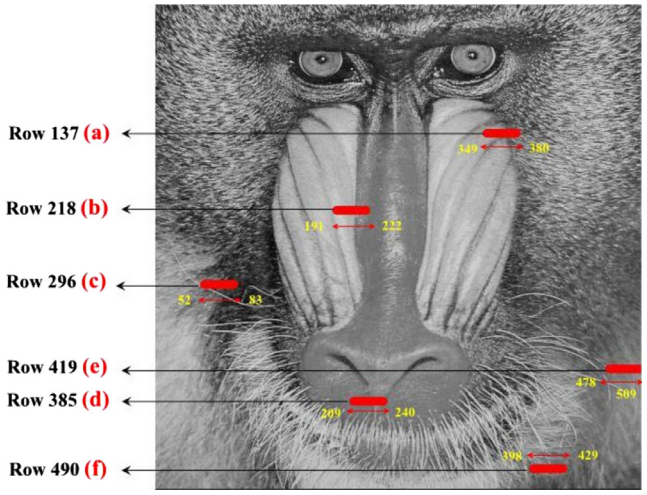

Fig. 4. "Baboon" gray-scale image of the size 512 × 512 pixels.

the reconstruction always converges to the original signal. However, the partial reconstructions from the proposed and Chebyshev moments, especially from the orders less than 10, are different.

We measured the reconstruction accuracy by the normalized mean square reconstruction error (NMSRE) defined as

$$NMSRE = \sqrt{\frac{\sum_{n=0}^{N-1}\left(f(n) - \tilde{f}(n)\right)^2}{\sum_{n=0}^{N-1} f^2(n)}}, \tag{43}$$

where $f(n)$ represents the original signal and $\tilde{f}(n)$ is its reconstructed version. The comparison of the reconstruction errors is presented in Fig. 9. It can be seen that the NMSRE for the proposed and Chebyshev moments are almost the same for the orders higher than 10.

5.3. Signal reconstruction from noisy data

Real signals are often corrupted by noise. Stable reconstruction of the original signal from the moments, which have been com-

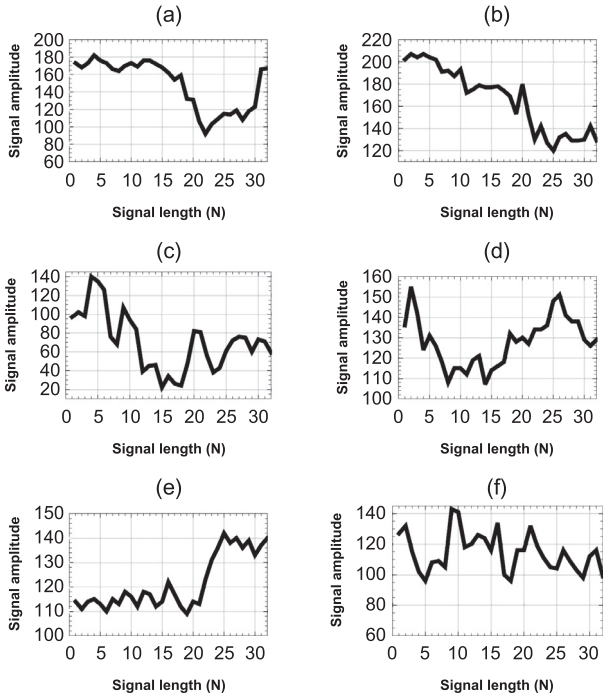

Fig. 5. The plots of six test signals extracted from the "Baboon" image: (a) row 137, columns from 349 to 380, (b) row 218, columns from 191 to 222, (c) row 296, columns from 52 to 83, (d) row 385, columns from 478 to 509, (e) row 419, columns from 209 to 240, (f) row 490, columns from 398 to 429.

Table 1
Confidence intervals for noise-free case shown in the form of $\mu \pm 1.96\frac{\sigma}{\sqrt{n}}$.

Order	Chebyshev moments	Proposed moments
2	(0.1306 ± 0.1160)	(0.2648 ± 0.1221)
4	(0.1000 ± 0.0939)	(0.1249 ± 0.0548)
6	(0.0814 ± 0.0705)	(0.0892 ± 0.0687)
8	(0.0748 ± 0.0719)	(0.0747 ± 0.0703)
10	(0.0721 ± 0.0701)	(0.0712 ± 0.0692)
12	(0.0609 ± 0.0597)	(0.0586 ± 0.0546)
14	(0.0551 ± 0.0551)	(0.0558 ± 0.0551)
16	(0.0453 ± 0.0387)	(0.0452 ± 0.0394)
18	(0.0395 ± 0.0302)	(0.0401 ± 0.0312)
20	(0.0366 ± 0.0263)	(0.0368 ± 0.0267)
22	(0.0334 ± 0.0223)	(0.0343 ± 0.0243)
24	(0.0299 ± 0.0188)	(0.0294 ± 0.0184)
26	(0.0239 ± 0.0182)	(0.0241 ± 0.0185)
28	(0.0211 ± 0.0157)	(0.0212 ± 0.0165)
30	(0.0117 ± 0.0052)	(0.0114 ± 0.0048)
32	(0.0000 ± 0.0000)	(0.0000 ± 0.0000)

puted from the noisy signal, is one of the most important indicators of suitability of the given type of moments for signal analysis. Signal reconstruction from noisy data is a difficult problem. Even if we had a perfect reconstruction algorithm, we would never obtain exactly the noise-free original signal. If we minimize the mean-square error between the reconstructed and noise-free original signals, we find out that an optimal order of moments exists. Moments of higher orders contribute more to reconstruction of the noise rather than to reconstruction of the signal. Since the problem is ill-posed, the reconstruction error from noisy data may be very high, even if we use this optimal moment order.

In this experiment, we used the same signals as before. We corrupted them by additive zero-mean white Gaussian noise such that the signal-to noise ratio was 25 dB (see Fig. 10 for the noisy signals). The reconstruction process and error measurement were analogous to the noise-free case. The reconstructed signals are

Table 2
Confidence intervals for noisy case shown in the form of $\mu \pm 1.96\frac{\sigma}{\sqrt{n}}$.

Order	Chebyshev moments	Proposed moments
2	(0.1569 ± 0.1108)	(0.2709 ± 0.1205)
4	(0.1455 ± 0.0816)	(0.1577 ± 0.0469)
6	(0.1418 ± 0.0593)	(0.1480 ± 0.0575)
8	(0.1487 ± 0.0567)	(0.1495 ± 0.0549)
10	(0.1506 ± 0.0525)	(0.1491 ± 0.0511)
12	(0.1536 ± 0.0387)	(0.1504 ± 0.0346)
14	(0.1545 ± 0.0350)	(0.1541 ± 0.0338)
16	(0.1589 ± 0.0287)	(0.1562 ± 0.0292)
18	(0.1692 ± 0.0386)	(0.1697 ± 0.0401)
20	(0.1725 ± 0.0379)	(0.1720 ± 0.0387)
22	(0.1749 ± 0.0341)	(0.1753 ± 0.0347)
24	(0.1845 ± 0.0483)	(0.1846 ± 0.0483)
26	(0.1889 ± 0.0493)	(0.1888 ± 0.0489)
28	(0.1975 ± 0.0448)	(0.1978 ± 0.0448)
30	(0.2034 ± 0.0454)	(0.2035 ± 0.0457)
32	(0.2156 ± 0.0511)	(0.2156 ± 0.0511)

plotted in Figs. 11–13. Like in the previous experiment, we can observe only little differences between the reconstructions from the proposed and the Chebyshev moments.

Fig. 14 shows the reconstruction errors by using Chebyshev moments and our proposed method. Similarly to the noise-free case, the differences for moment orders higher than 10 are insignificant. Hence, the noise robustness of both moment families is comparable and sufficiently high in both cases. For low-order reconstruction, there are domains where one method outperforms the other one. This is, however, substantially dependent on the signal itself and cannot be generalized into a signal-independent statement. In Fig. 14, we can observe the phenomenon of optimal moment order p_{opt}, which corresponds to the local minimum of the NMSRE curve. Order p_{opt} depends on the data but also on the SNR – the higher SNR (i.e. the less noise), the higher p_{opt}. For SNR approaching infinity we obtain $p_{opt} = N$.

5.4. Confidence intervals of reconstruction error

Confidence intervals consist of a range of values that act as good estimates of the unknown parameter; however, the interval computed from a particular sample does not necessarily include the true value of the parameter. The desired level of confidence is a user-defined parameter, it is not determined by data. If a corresponding hypothesis test is performed, the confidence level is the complement of respective level of significance, i.e. a 95% confidence interval reflects a significance level of 0.05. Here, we use a confidence level of 95% for our both noise-free and noisy experiments due to the calculated reconstruction errors. This level of confidence can be formulated by $\mu \pm 1.96\frac{\sigma}{\sqrt{n}}$ where μ is the mean of NMSRE, σ is the standard deviation of NMSRE and n is the number of test signals (in this case $n = 6$). The confidence intervals of the NMSRE for all moment orders are shown in Tables 1 and 2 for noise-free and noisy cases, respectively.

5.5. Time complexity of moment computation

In this experiment, a one dimensional signal is used to measure the speed of the moment computation by applying the hypergeometric and recursive methods for discrete Chebyshev and the proposed polynomials. The signal of length $N = 128$ used in this test was generated as

$$f(n) = sinc\left(\frac{n}{2}\right)$$

for $0 \le n \le 127$ (see Fig. 15 for the plot).

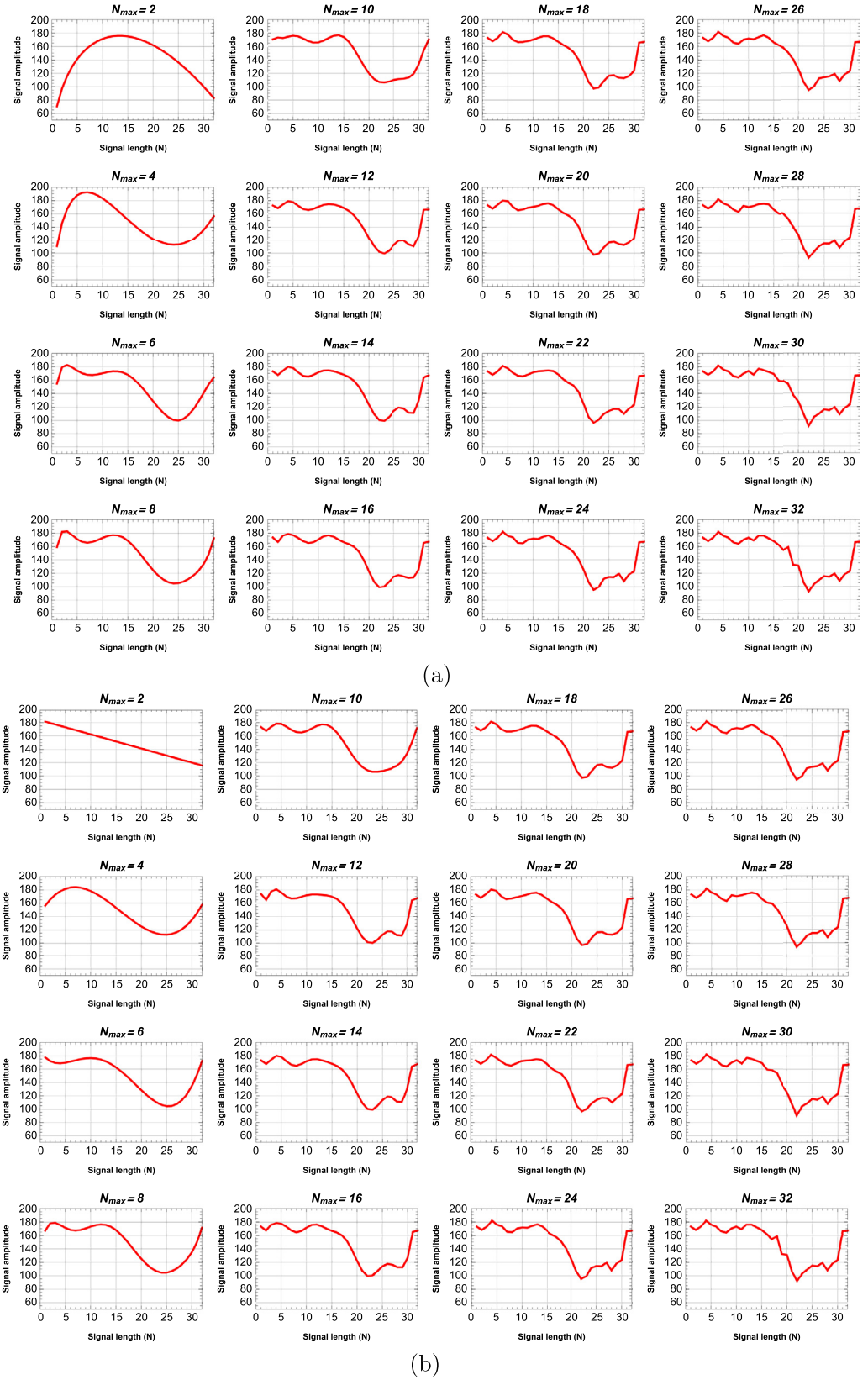

Fig. 6. Signal reconstruction of Fig. 5(a): (a) the proposed moments and (b) discrete Chebyshev moments.

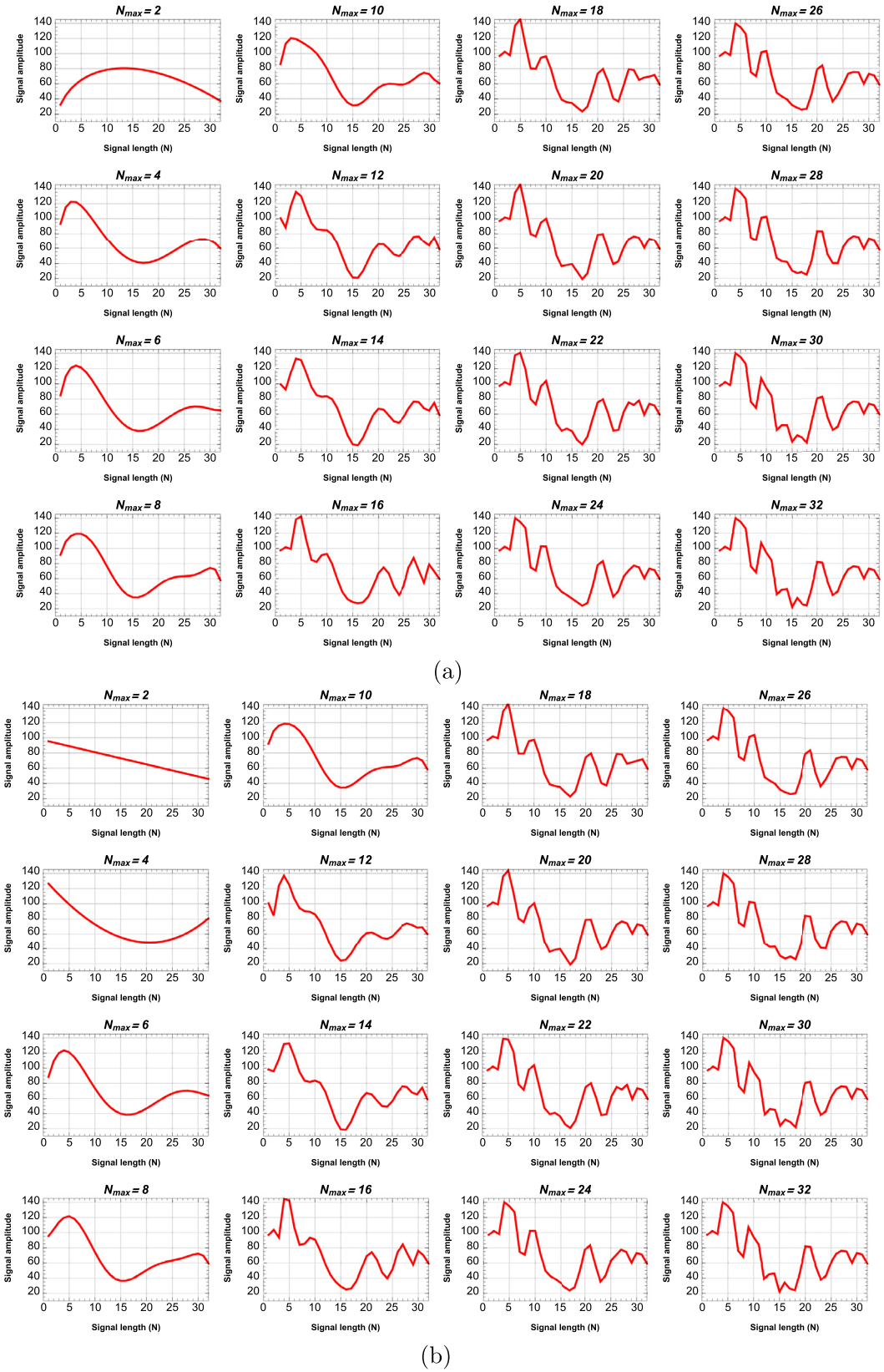

Fig. 7. Signal reconstruction of Fig. 5(c): (a) the proposed moments and (b) discrete Chebyshev moments.

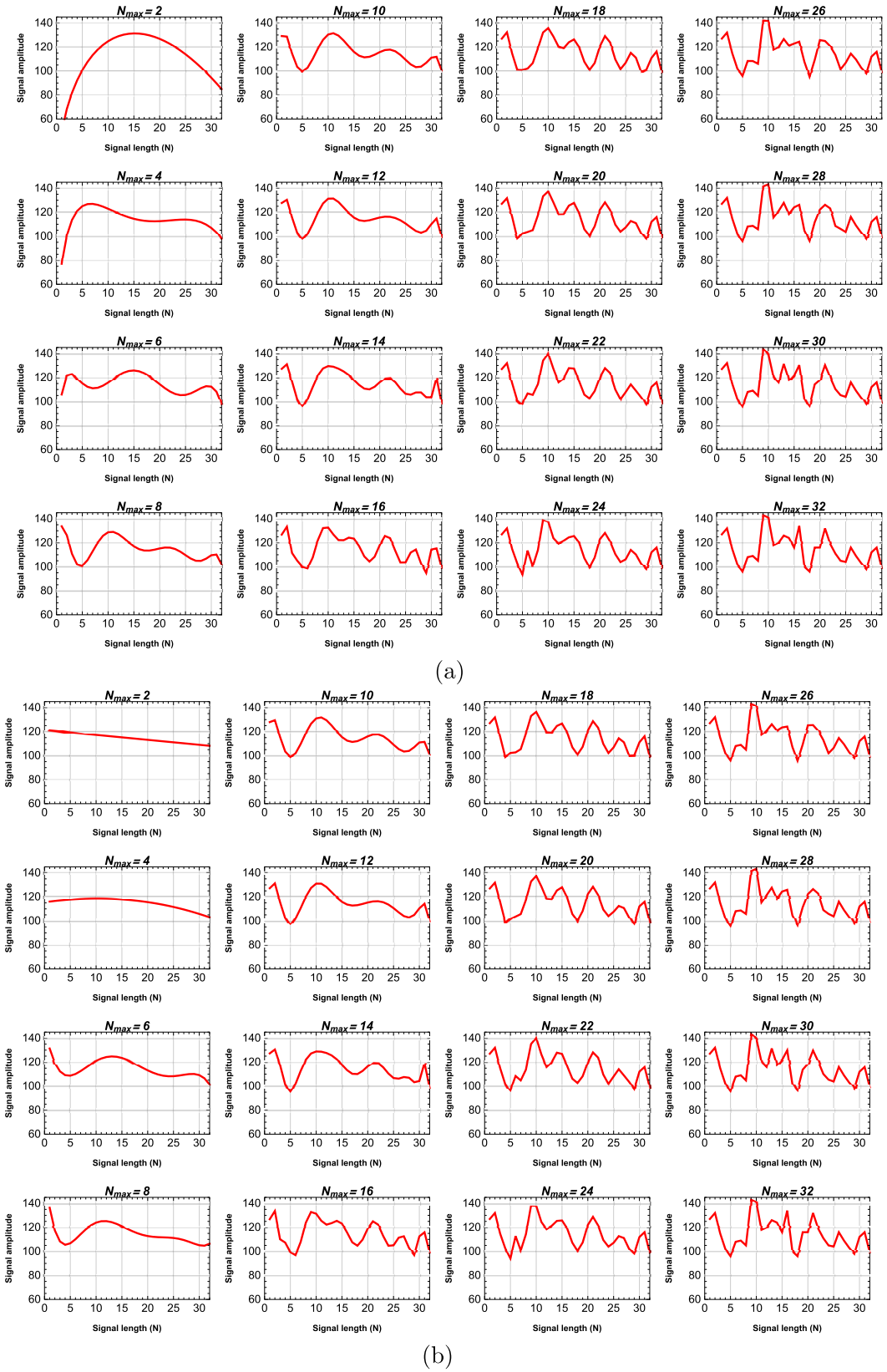

Fig. 8. Signal reconstruction of Fig. 5(f): (a) the proposed moments and (b) discrete Chebyshev moments.

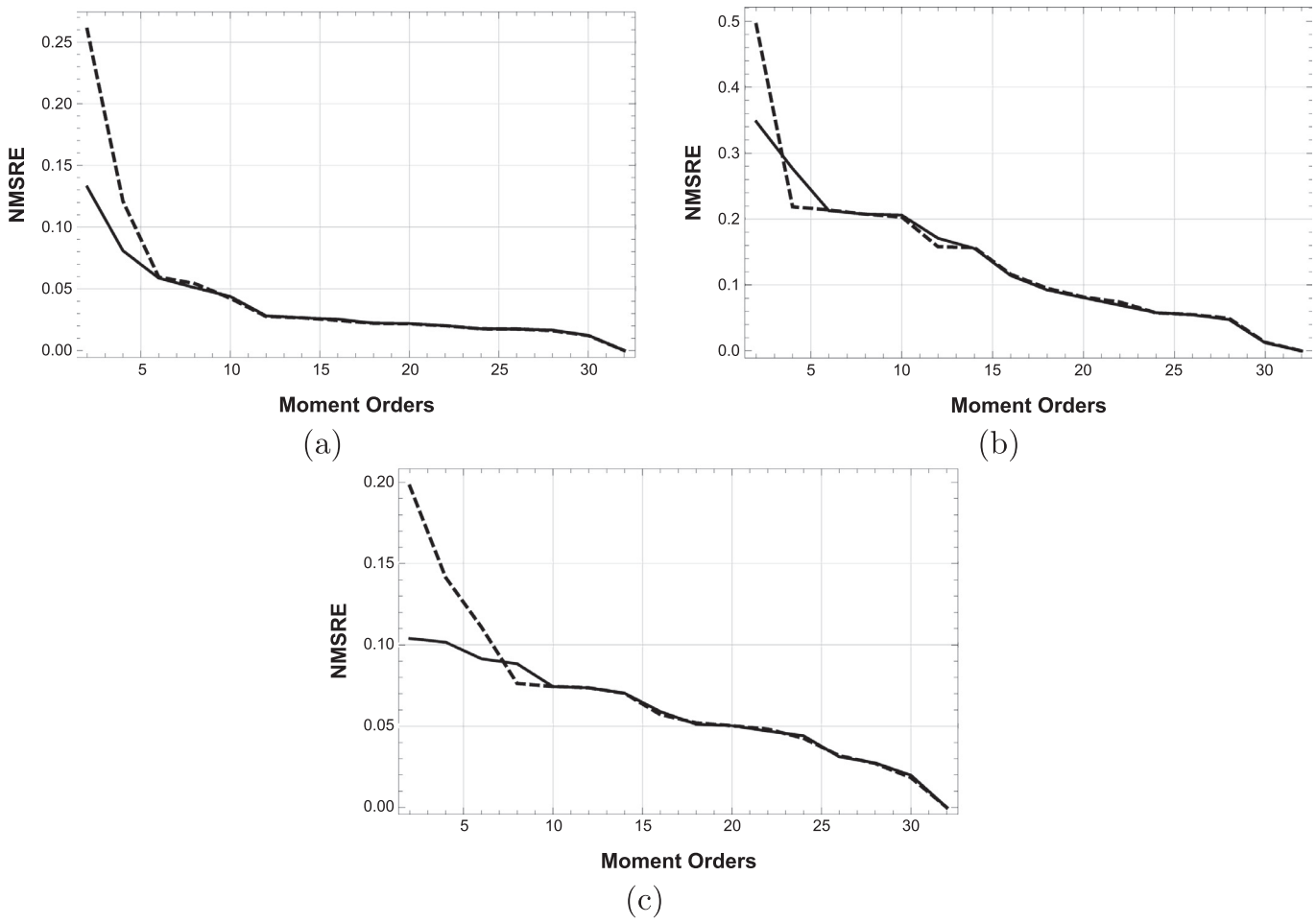

Fig. 9. Reconstruction error for Figs. 6–8: The proposed moments (dashed line) and discrete Chebyshev moments (solid line).

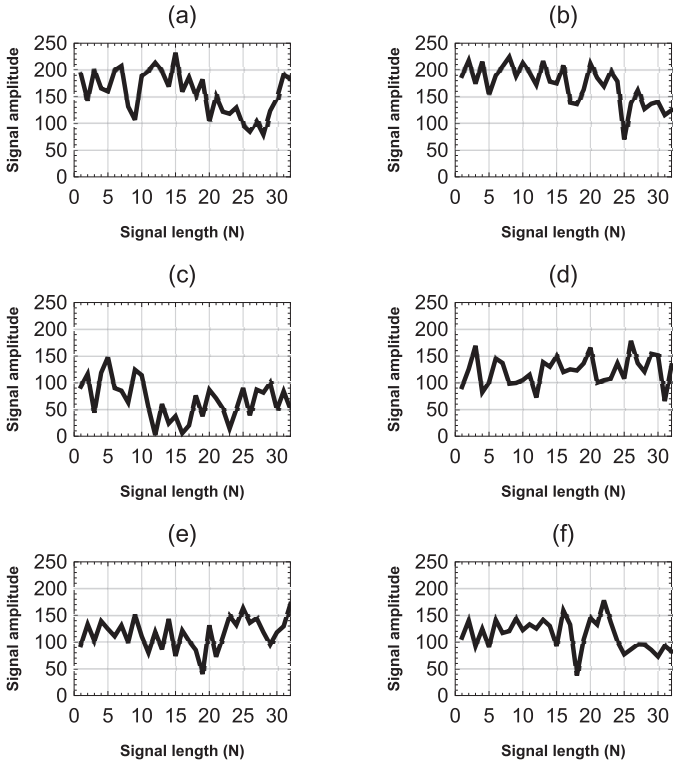

Fig. 10. Noisy signals of Fig. 5 corrupted by additive zero-mean white Gaussian noise of SNR = 25 db.

Table 3
Average CPU elapsed times in milliseconds for computation of Chebyshev and the proposed moments using two different methods.

Order of moments	Hypergeometric method		Recursive method	
	Chebyshev moments	Proposed moments	Chebyshev moments	Proposed moments
0	0.23	0.25	0.07	0.12
10	0.47	0.59	0.19	0.34
20	0.86	0.94	0.54	0.68
30	1.27	1.35	0.87	1.13
40	3.16	3.34	1.06	1.44
50	5.07	5.27	1.89	2.32
75	9.80	11.66	3.67	5.83
100	24.69	31.12	7.72	10.25
125	75.88	90.32	16.11	23.43

Each moment was calculated four times and the average CPU elapsed time was stored. Table 3 shows the average times measured in this experiment. We can see that the recursive method is much faster than the hypergeometric one in all cases, so there is a clear recommendation to use recursive formulas for implementation. On the other hand, there is no significant differences between the complexity of the proposed and Chebyshev moments.

6. Conclusion

A new set of discrete orthogonal moment features based on a new class of a one-parameter family of DOPs established by the UFIR functions earlier derived by Shmaliy has been proposed in

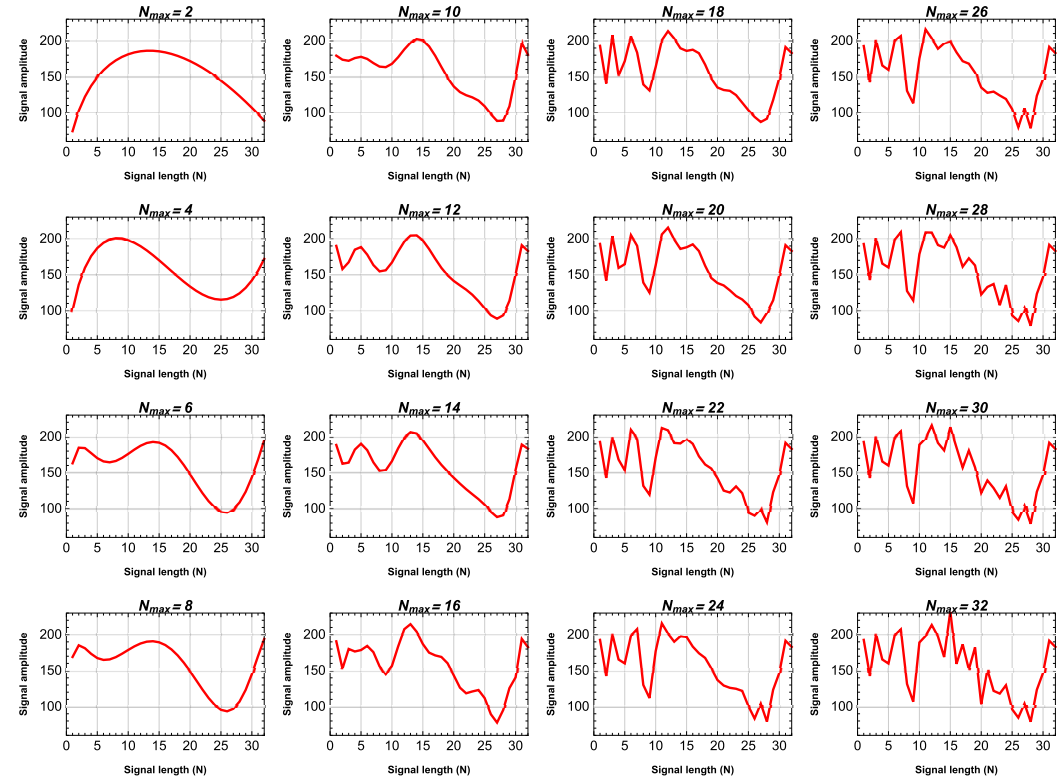

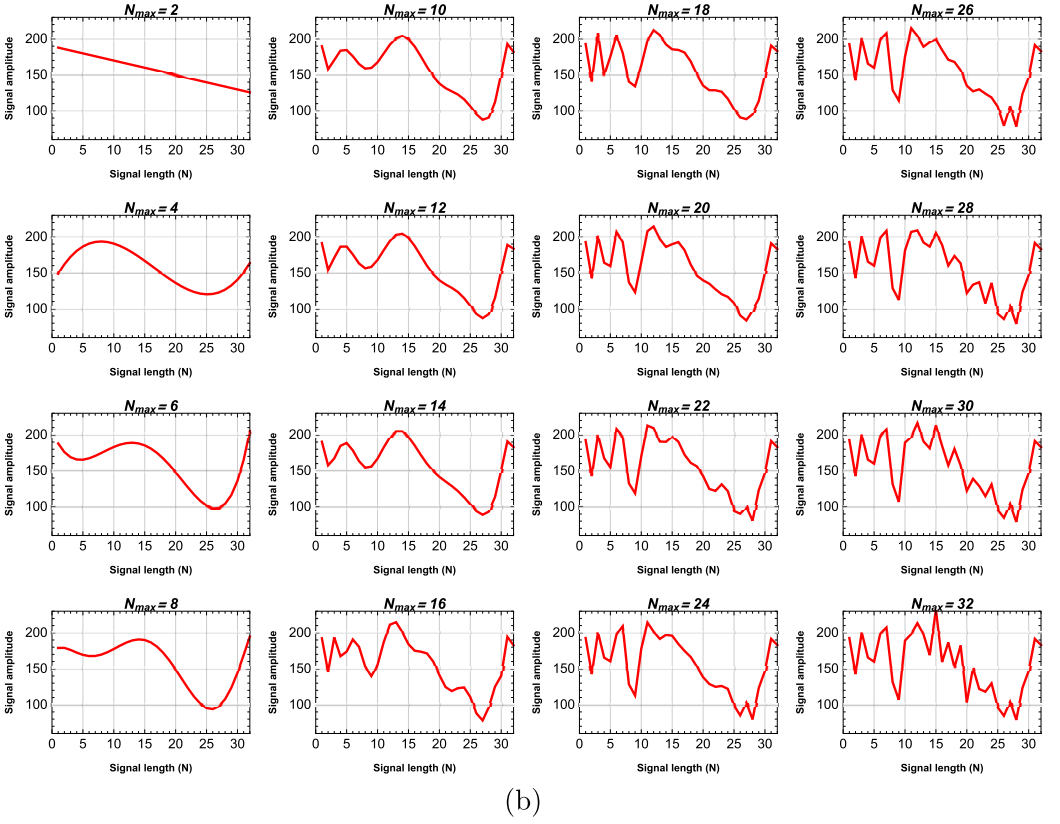

Fig. 11. Signal reconstruction of Fig. 5(a): (a) The proposed moments and (b) discrete Chebyshev moments.

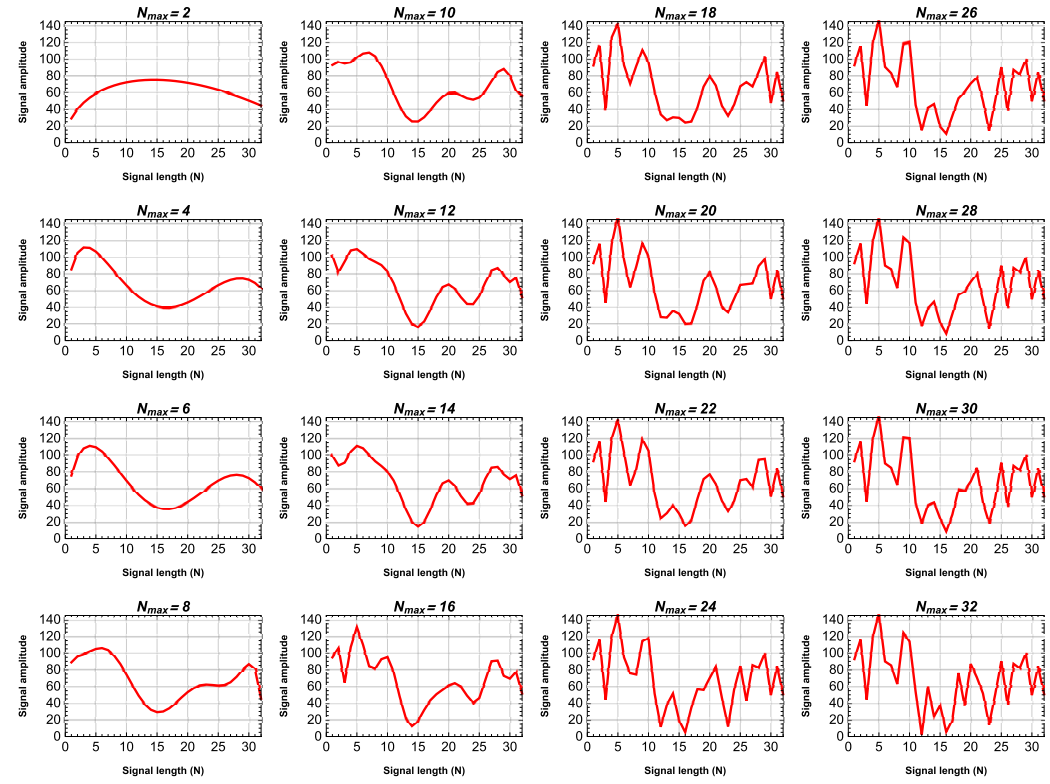

(a)

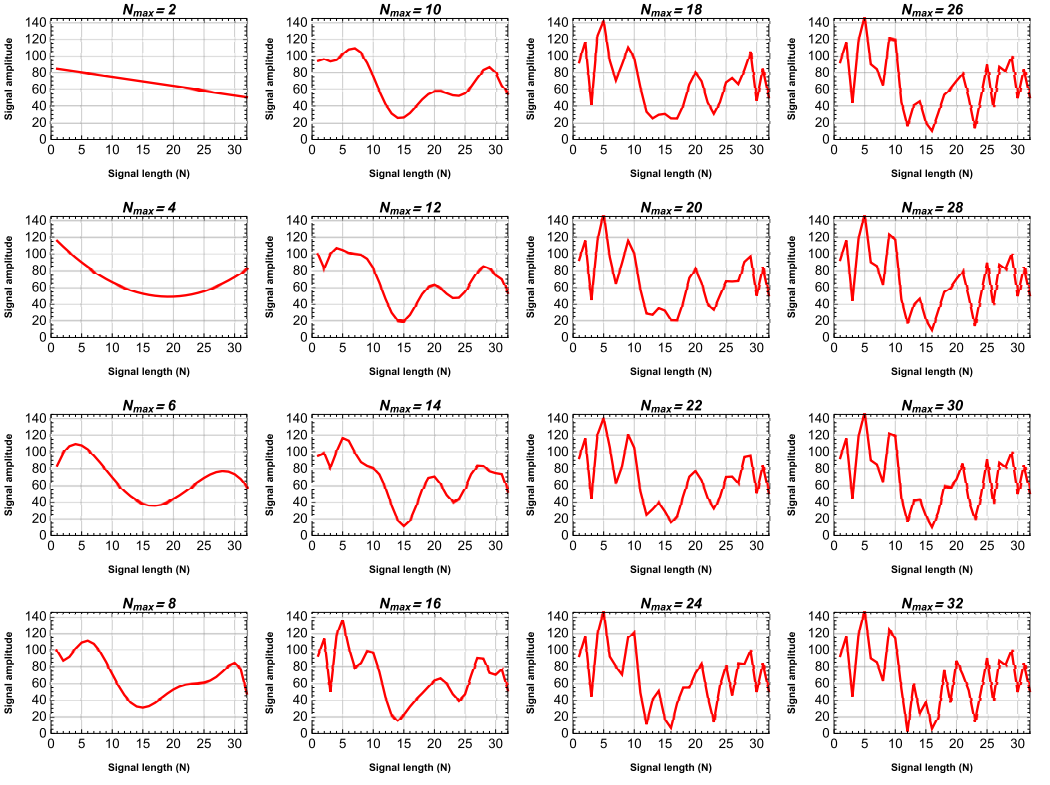

(b)

Fig. 12. Signal reconstruction of Fig. 5(c): (a) The proposed moments and (b) discrete Chebyshev moments.

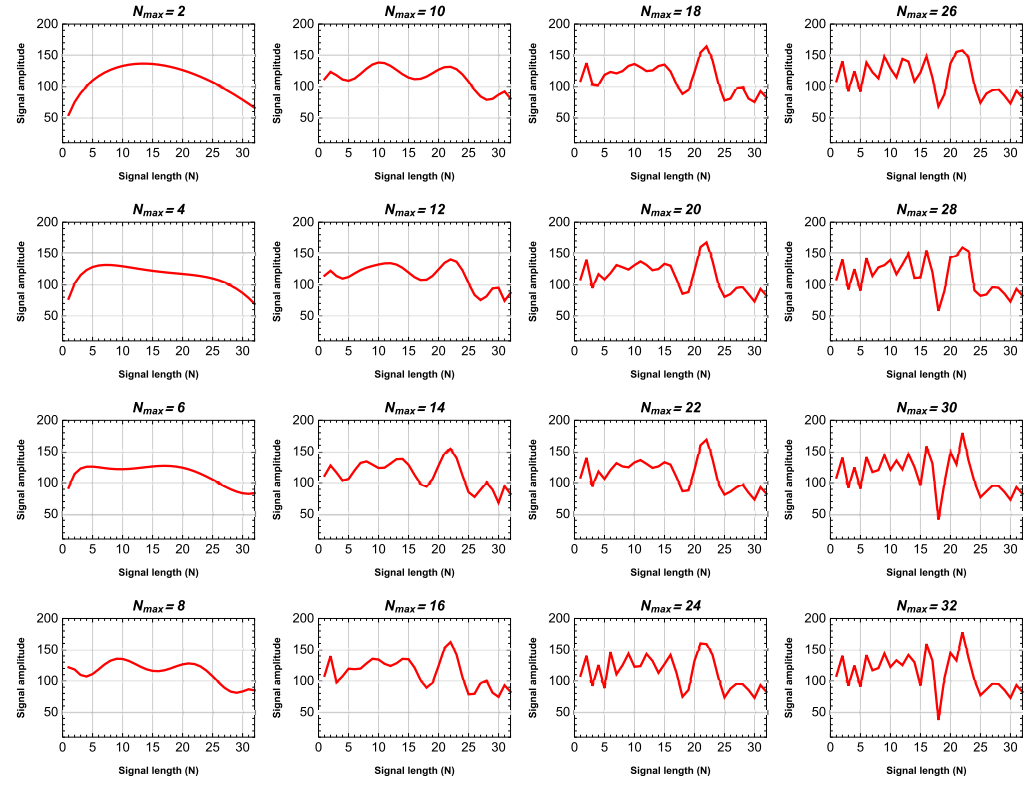

(a)

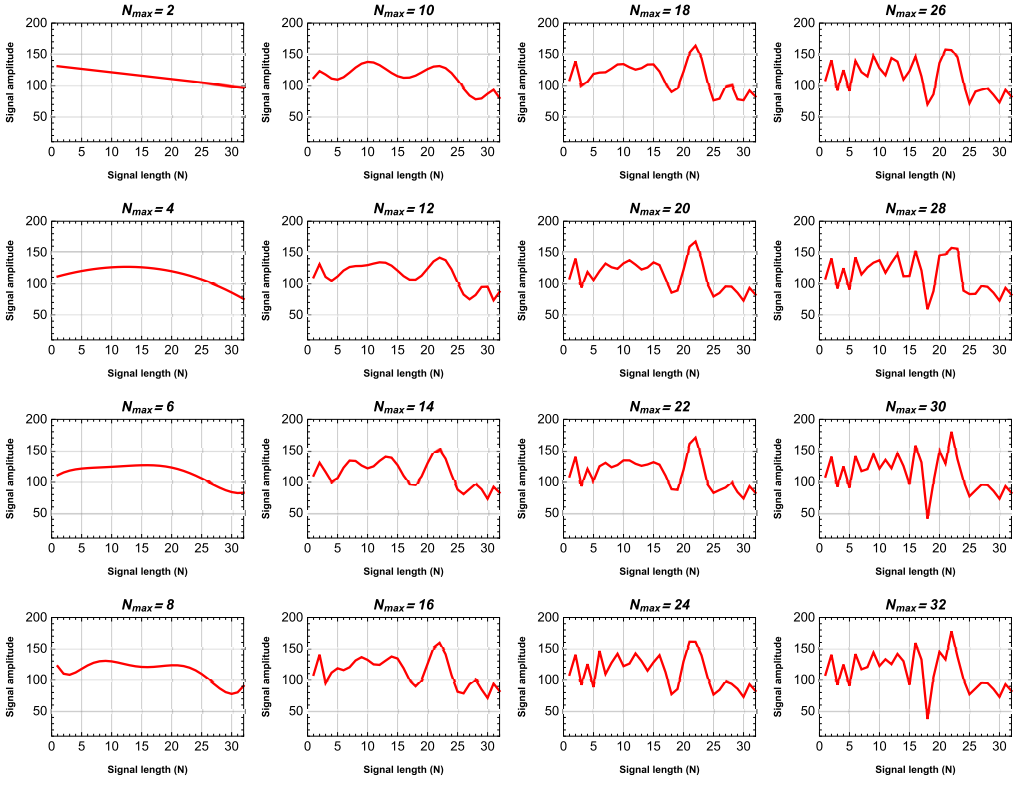

(b)

Fig. 13. Signal reconstruction of Fig. 5(f): (a) The proposed moments and (b) discrete Chebyshev moments.

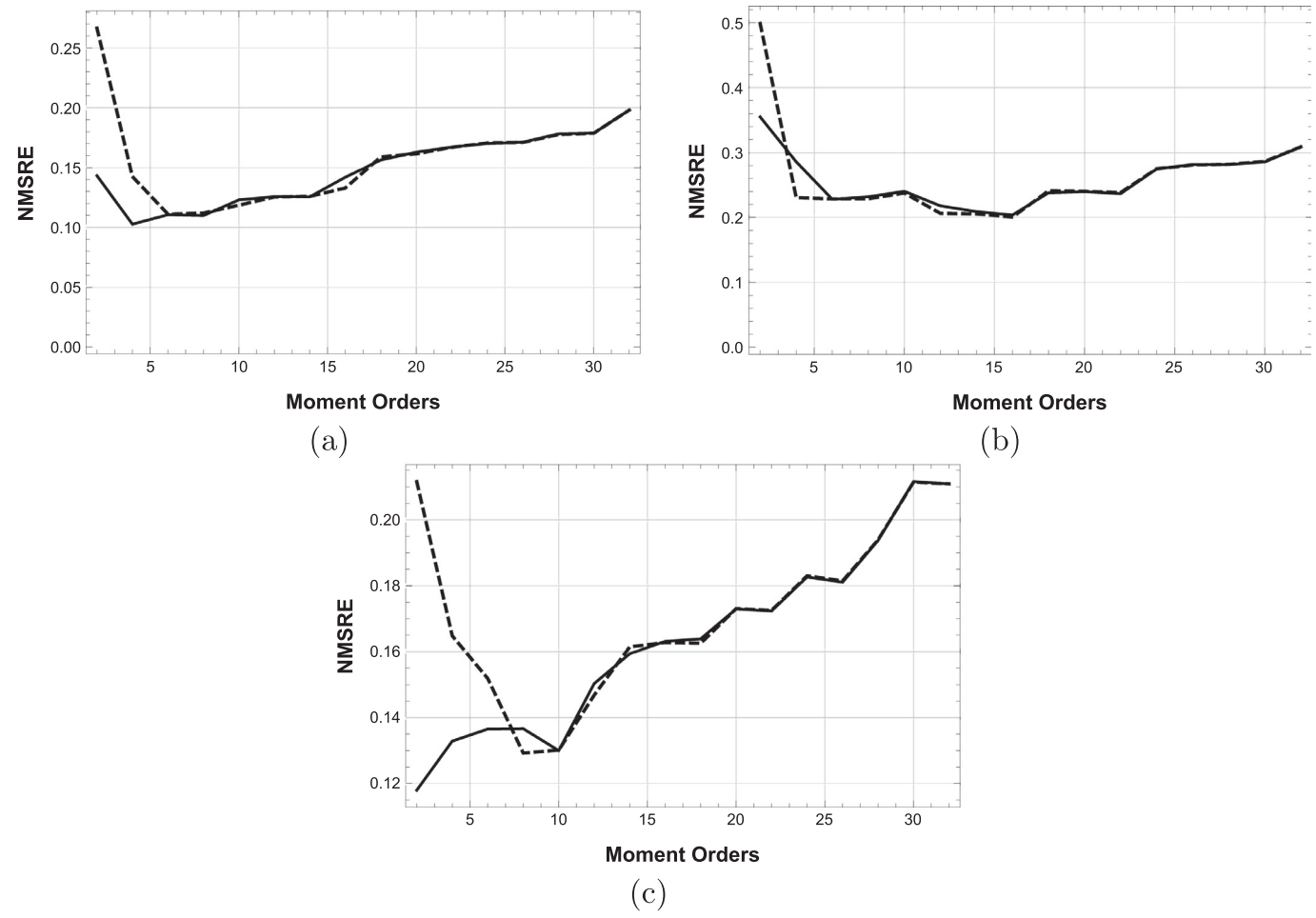

Fig. 14. Reconstruction error for Figs. 11–13: Proposed moments (dashed line) and Chebyshev moments (solid line). The minimum indicates the moment order which is optimal for signal reconstruction.

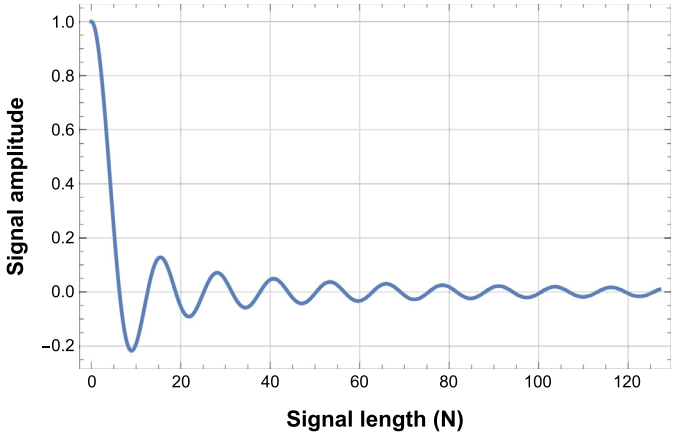

Fig. 15. The test signal of length 128 used for the measurement of the moment calculation time complexity.

this paper. The new DOPs have two remarkable features. In a contrast to many popular DOPs such as Krawtchouk and Hahn, they depend on a single parameter (the signal length) only. The second distinction is that they are orthogonal with respect to linear weight function, while most of other polynomials require symmetric non-linear weight functions. We derived both explicit formulas to compute these new class of DOPs based on the discrete Rodrigues' representation and hypergeometric form, respectively. The hypergeometric representation of these polynomials has not been known before. We also showed that the new DOPs are the discrete version of the radial Mellin polynomials in the limiting case when the length of the signal approaches infinity.

After employing Z-transform to find a straightforward solution for the proposed DOPs, we applied the new discrete moments to signal analysis, particularly to signal reconstruction. Experimental results conclusively prove the effectiveness of the proposed moments as a new feature descriptors. Comparative analysis with Chebyshev moments, which form another single-parameter family, shows the capability of the proposed moments in terms of reconstruction error of noise-free/noisy signals.

This paper studied only 1D polynomials and moments. Extension into 2D and 3D is straightforward – we can define the multivariate polynomials as products of the univariate ones in each dimension. Doing so, we can study the performance of the new moments in all traditional tasks of 2D and 3D image analysis, where moments have been commonly applied [22] – in object description and recognition, watermarking, image registration, and many others. This could be a subject of a future work.

Acknowledgment

The authors thank the Czech Science Foundation for financial support under the Grant No. GA15 – 16928S. Barmak Honarvar was also supported by the Czech Academy of Sciences under the PPLZ framework program. Jan Flusser thanks the Joint Laboratory SALOME 2 for non-financial support.

Appendix A

Derivation of Eq. (25). Let

$$h_p(n,N) \overset{\mathscr{Z}}{\longleftrightarrow} H_p(z)\ ;\ ng(n,p) = y_p(n) \overset{\mathscr{Z}}{\longleftrightarrow} Y_p(z).$$

The generalization of forward difference yields

$$\Delta^p\{y_p(n)\} = \sum_{k=0}^{p}(-1)^{p-k}\binom{p}{k}y_p(n+k). \tag{A.1}$$

By time shifting and using differentiation properties in Z domain, we obtain

$$nh_p(n,N) \overset{\mathscr{Z}}{\longleftrightarrow} -z\frac{\mathrm{d}H_p(z)}{\mathrm{d}z}, \tag{A.2}$$

$$\Delta^p\{y_p(n)\} \overset{\mathscr{Z}}{\longleftrightarrow} \sum_{k=0}^{p}(-1)^{p-k}\binom{p}{k}z^kY_p(z). \tag{A.3}$$

Combining (A.2) and (A.3) leads us to (25).

Appendix B

Comparing Eq. (12) as low-order polynomials and (35) allows us to find $\sigma(p, N)$. Table B-1 shows the first four low-order polynomials and their corresponding $\sigma(p, N)$ explicitly. The third column of this table shows that the numerators include Pochhammer numbers multiplied by the factorial of the degree p. The denominators equal $p+1$.

Table B-1
Explicit formula to find $\sigma(p, N)$.

p	$h_p(n, N)$	$\sigma(p, N)$
0	$h_0(n,N) = \frac{1}{N}$	N
1	$h_1(n,N) = \frac{-6n+2(2N-1)}{N(N+1)}$	$\frac{N(N+1)}{2}$
2	$h_2(n,N) = \frac{30n^2-18(2N-1)n+3(3N^2-3N+2)}{N(N+1)(N+2)}$	$\frac{2N(N+1)(N+2)}{3}$
3	$h_3(n,N) = \frac{-140n^3+120(2N-1)n^2-20(6N^2-6N+5)n+8(2N^3-3N^2+7N-3)}{N(N+1)(N+2)(N+3)}$	$\frac{6N(N+1)(N+2)(N+3)}{4}$
⋮	⋮	⋮
p	$\sum_{i=0}^{p}(-1)^i\frac{M^{(p)}_{(i+1),1}(N)}{\lvert H_p(N)\rvert}n^i$	$\frac{p!(N)_{p+1}}{p+1}$

Appendix C

Proof of Theorem 1: We expand (33) using the general expansion formula of the forward difference (23) as

$$h_p(n,N) = \frac{p+1}{np!(N)_{p+1}}\sum_{k=0}^{p}(-1)^{p-k}\binom{p}{k}(n+k) \times (n+k-p)_p(N-n-k)_p. \tag{C.1}$$

The main part of the proof is to convert each term in the above sum to a form of Pochhammer symbol as $(.)_k$. We use the following well-known properties of Gamma function and Pochhammer symbol for integer variables n and k

$$\Gamma(n+1) = n! \tag{C.2a}$$

$$(n)_k = \frac{\Gamma(n+k)}{\Gamma(n)} \tag{C.2b}$$

$$\Gamma(n+k) = \Gamma(n)(n)_k \tag{C.2c}$$

$$\Gamma(n-k) = \frac{(-1)^k\Gamma(n)}{(1-n)_k} \tag{C.2d}$$

By expanding $\binom{p}{k}$ as $\frac{p!}{k!(p-k)!}$ and using (C.2 b), Eq. (C.1) can be rewritten as

$$h_p(n,N) = \frac{(p+1)(-1)^p}{np!(N)_{p+1}}\sum_{k=0}^{p}(-1)^{-k}\frac{p!}{k!(p-k)!}(n+k) \times \frac{\Gamma(n+k)}{\Gamma(n+k-p)}\frac{\Gamma(N-n-k+p)}{\Gamma(N-n-k)}. \tag{C.3}$$

To obtain a Pochhammer symbol expression for terms $(n+k)$ and $(p-k)!$, we use the identities (C.2) which leads to

$$n+k = \frac{(n+k)!}{(n+k-1)!} = \frac{\Gamma(n+k+1)}{\Gamma(n+k)} = n\frac{(n+1)_k}{(n)_k} \tag{C.4a}$$

$$(p-k)! = \Gamma(p-k+1) = \frac{(-1)^k\Gamma(p+1)}{(1-p-1)_k} = \frac{(-1)^kp!}{(-p)_k} \tag{C.4b}$$

Substituting (C.4) into (C.3) and using (C.2), (C.3) can be further simplified into the form

$$h_p(n,N) = \frac{(p+1)(-1)^p}{np!(N)_{p+1}}\sum_{k=0}^{p}(-1)^{-k}\frac{p!}{k!\frac{(-1)^kp!}{(-p)_k}}n\frac{(n+1)_k}{(n)_k} \times \frac{\Gamma(n)(n)_k}{\Gamma(n-p)(n-p)_k}\frac{(-1)^k\Gamma(N-n+p)}{(1-N+n-p)_k}\frac{(1-N+n)_k}{(-1)^k\Gamma(N-n)}. \tag{C.5}$$

After some manipulations, (C.5) becomes

$$h_p(n,N) = \frac{(-1)^p(p+1)(n-p)_p(N-n)_p}{p!(N)_{p+1}}\sum_{k=0}^{p}\frac{1}{k!} \times \frac{(-p)_k(n+1)_k(1-N+n)_k}{(n-p)_k(1-N-p+n)_k}. \tag{C.6}$$

Introducing hypergeometric function ${}_3F_2$ into the above equation, we finally end up with Eq. (34), which completes the proof of Theorem 1.

References

[1] K. Jordán, Calculus of Finite Differences, AMS Chelsea Publishing Series, Chelsea Publishing Company, 1965.

[2] A.F. Nikiforov, V.B. Uvarov, S.K. Suslov, Classical Orthogonal Polynomials of a Discrete Variable, Springer Berlin Heidelberg, Berlin, Heidelberg, pp. 18–54. 10.1007/978-3-642-74748-9_2

[3] R. Mukundan, S. Ong, P. Lee, Image analysis by Tschebichef moments, Image Process. IEEE Trans. 10 (9) (2001) 1357–1364.

[4] W.A. Jassim, R. Paramesran, M.S.A. Zilany, Enhancing noisy speech signals using orthogonal moments, IET Signal Process. 8 (8) (2014) 891–905, doi:10.1049/iet-spr.2013.0322.

[5] G.A. Papakostas, D.A. Karras, B.G. Mertzios, Image coding using a wavelet based Zernike moments compression technique, in: Digital Signal Processing, 2002. DSP 2002. 2002 14th International Conference on,, 2, 2002, pp. 517–520, doi:10.1109/ICDSP.2002.1028141.

[6] G. Mandyam, N. Ahmed, The discrete Laguerre transform: derivation and applications, IEEE Trans. Signal Process. 44 (12) (1996) 2925–2931, doi:10.1109/78.553468.

[7] M.R. Teague, Image analysis via the general theory of moments, J. Opt. Soc. Am. 70 (8) (1980) 920–930, doi:10.1364/JOSA.70.000920.

[8] J. Flusser, B. Zitova, T. Suk, Moments and Moment Invariants in Pattern Recognition, Wiley Publishing, 2009.

[9] P.L.R. Mukundan, S.H. Ong, Discrete vs. continuous orthogonal moments for image analysis, in: International Conference on Imaging Science, Systems and Technology-CISST01, 2001, pp. 23–29.

[10] Y.S. Shmaliy, An unbiased FIR filter for TIEmodel of a local clock in applications to GPS-based timekeeping, IEEE Trans. Ultrason. Ferroelectr. Freq. Control 53 (5) (2006) 862–870, doi:10.1109/TUFFC.2006.1632677.

[11] H. Gamboa-Rosales, L.J. Morales-Mendoza, Y.S. Shmaliy, A new class of discrete orthogonal polynomials for blind fitting of finite data, in: Electrical Engineering, Computing Science and Automatic Control (CCE), 2013 10th International Conference on, 2013, pp. 185–190, doi:10.1109/ICEEE.2013.6676049.

[12] Y.S. Shmaliy, L.J. Morales-Mendoza, FIR smoothing of discrete-time polynomial signals in state space, IEEE Trans. Signal Process. 58 (5) (2010) 2544–2555, doi:10.1109/TSP.2010.2041595.

[13] Y.S. Shmaliy, Optimal gains of FIR estimators for a class of discrete-time state-space models, IEEE Signal Process. Lett. 15 (2008) 517–520, doi:10.1109/LSP.2008.925746.
[14] P. Heinonen, Y. Neuvo, FIR-median hybrid filters with predictive FIR substructures, IEEE Trans. Acoust. Speech Signal Process. 36 (6) (1988) 892–899, doi:10.1109/29.1600.
[15] H. Hamboa-Rosales, L. Morales-Mendoza, Y.S. Shmaliy, Unbiased impulse responses-a class of discrete orthogonal polynomials, ICIC Express Lett. 7 (7) (2013) 2005–2010.
[16] L.J. Morales-Mendoza, H. Gamboa-Rosales, Y.S. Shmaliy, A new class of discrete orthogonal polynomials for blind fitting of finite data, Signal Process. 93 (7) (2013) 1785–1793. http://dx.doi.org/10.1016/j.sigpro.2013.01.023.
[17] Image reconstruction method based on discrete orthogonal moments, 2014, CN Patent App. CN 201,410,374,455.
[18] K. Holmåker, On a Discrete Rodrigues' Formula and a Second Class of Orthogonal Hahn Polynomials, Department of Mathematics, Chalmers University of Technology and Göteborg University, Department of Mathematics, Chalmers University of Technology, 1977.
[19] N.J.A. Sloane, S. Plouffe, The Encyclopedia of Integer Sequences, xiii, Academic Press, San Diego, 1995, p. 587. ISBN 0-12-558630-2).
[20] M. Abramowitz, Handbook of Mathematical Functions, With Formulas, Graphs, and Mathematical Tables, Dover Publications, Incorporated, 1974.
[21] Y. Sheng, L. Shen, Orthogonal Fourier-Mellin moments for invariant pattern recognition, J. Opt. Soc. Am. A 11 (6) (1994) 1748–1757, doi:10.1364/JOSAA.11.001748.
[22] J. Flusser, T. Suk, B. Zitova, 2D and 3D Image Analysis by Moments, Wiley, 2016.